

1 **Graphene oxide and Gold nanoparticle based dual platform with short DNA probe for the**
2 **PCR free DNA biosensing using Surface Enhance Raman Scattering**

3 Ibrahim Khalil,^a Wageeh A. Yehye,^{a,*} Nurhidayatullaili Muhd Julkapli,^a Shahrooz Rahmati,^a
4 Abu Ali Ibn Sina,^b Wan Jeffrey Basirun ^{a,c}, Mohd Rafie Johan ^a

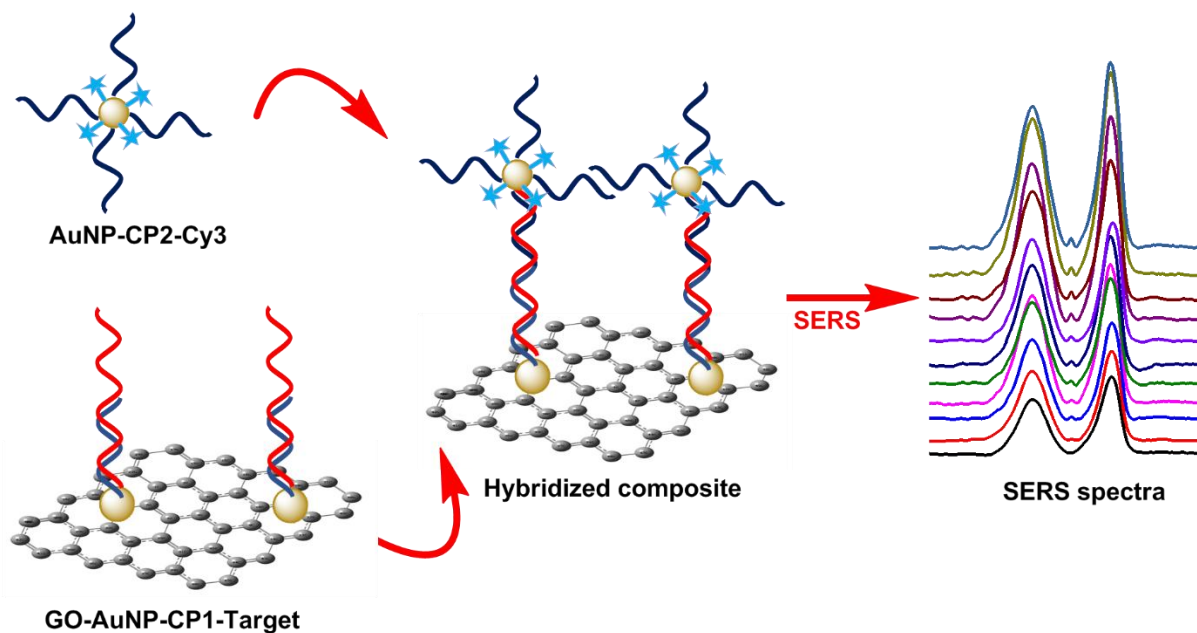
5
6 ^aNanotechnology & Catalysis Research Centre (NANOCAT), Institute of Graduate Studies,
7 University of Malaya, Kuala Lumpur 50603, Malaysia.

8 ^bCentre for Personalised Nanomedicine, Australian Institute for Bioengineering and
9 Nanotechnology (AIBN), Corner of College and Cooper Roads (Bldg 75), The University of
10 Queensland, Brisbane QLD 4072, Australia

11 ^cDepartment of Chemistry, Faculty of Science, University of Malaya, Kuala Lumpur 50603,
12 Malaysia.

13
14 *Corresponding author: wdabdoub@um.edu.my (W.A.Yehye),
15 Tel.: +603 7967 6954; Fax: +603 7967 6556

16
17 **Graphical Abstract**



18
19

20 **Abstract**

21 Surface-enhanced Raman scattering (SERS) based DNA biosensors have considered as
22 excellent, fast and ultrasensitive sensing technique which relies on the fingerprinting ability
23 to produce molecule specific distinct spectra. Unlike conventional fluorescence based
24 strategies SERS provides narrow spectral bandwidths, fluorescence quenching and
25 multiplexing ability, and fitting attribute with short length probe DNA sequences. Herein, we
26 report a novel and PCR free SERS based DNA detection strategy involving dual platforms and
27 short DNA probes for the detection of endangered species, Malayan Box Turtle (MBT)
28 (*Cuora amboinensis*). In this biosensing feature, the detection is based on the covalent
29 linking of the two platforms involving graphene oxide-gold nanoparticles (GO-AuNPs)
30 functionalized with capture probe 1 and gold nanoparticles (AuNPs) modified with capture
31 probe 2 and Raman dye (Cy3) via hybridization with the corresponding target sequences.
32 Coupling of the two platforms generates locally enhanced electromagnetic field 'hot spot',
33 formed at the junctions and interstitial crevices of the nanostructures and consequently
34 provide significant amplification of the SERS signal. Therefore, employing the two SERS
35 active substrates and short-length probe DNA sequences, we have managed to improve the
36 sensitivity of the biosensors to achieve a lowest limit of detection (LOD) as low as 10 fM.
37 Furthermore, the fabricated biosensor exhibited sensitivity even for single nucleotide base-
38 mismatch in the target DNA as well as showed excellent performance to discriminate closely
39 related six non-target DNA sequences. Although the developed SERS biosensor would be an
40 attractive platform for the authentication of MBT from diverse samples including forensic
41 and/or archaeological specimens, it could have universal application for detecting gene
42 specific biomarkers for many diseases including cancer.

43

44 **Keywords:** Graphene oxide-gold nanoparticles, surface-enhanced Raman scattering, DNA
45 biosensor, Sandwich biosensor, short-length DNA probe, Malayan Box Turtle.

46

47 **1. Introduction**

48 DNA sensing technology has rapidly emerged since last decades to get the biological
49 footprints of every species. Current technologies for DNA identification such as sequencing,
50 microarray and mass spectrometry are labor-intensive, time-consuming and require
51 expensive equipment. In addition, the use of short length DNA probe in the widely accepted

52 PCR based techniques (e.g. sequencing) for the DNA biosensing is often very challenging
53 (Ngo et al. 2016). While short-length amplicons, typically ≤ 150 bp in length improve the
54 better recovery of the detection from the degraded DNA specimens or compromised
55 forensic evidence (Turna et al. 2010), reduction of amplicon length in PCR based technique
56 is limited by low specificity, producing artifacts in the final results (Ali et al. 2012; Hird et al.
57 2006). Therefore, nanoparticles based DNA sensing has recently considered as one of the
58 best alternatives to the conventional strategies to conserve the high specificity and
59 sensitivity using very short segment of DNA as the detection probe (Merkoçi 2010). In recent
60 years, nanoparticles based DNA biosensors are employed in diversified applications
61 including identification of pathogenic microorganisms (Tondro et al. 2018), detection of
62 cancer biomarkers (Huang et al. 2018; Shahrokhian and Salimian 2018), trace elements,
63 environmental hazards, drug screening, and the analysis of gene sequences (Li et al. 2005;
64 Saidur et al. 2017) and food safety (Ha et al. 2017). Thus we believe that nanoparticle based
65 DNA sensing technology (e.g. SERS) could be strategic to identify the endangered species
66 such as Malayan box turtle (MBT). MBT is an endangered and vulnerable turtle species but
67 an attractive item to the illegal wildlife trader due to its huge appeal as an exotic food item
68 and in traditional medicine. Moreover, MBT is a natural scavenger of waste materials, hence
69 carrier of several pathogenic microorganisms, parasites, various toxins, and heavy metals
70 (Ali et al. 2016; Green et al. 2010). Therefore, consumption of or contact with this turtle
71 and/or turtle-derived materials in food chains and medicines have significant health
72 concerns which urge for the reliable authentication technique for this turtle species to
73 restrict health hazards, as well as to prevent or reduce illegal trades.

74 SERS has emerged as the most powerful analytical technique for the fast and ultra-
75 sensitive detection of DNA with single molecule differentiations by providing intrinsic
76 chemical information and vibrational fingerprints of each molecules (Nie and Emory 1997;
77 Xu et al. 2015). It has certain advantages over fluorescence, spectroscopic, electrochemistry
78 and some other techniques. For instance, no photo-bleaching from the Raman tags or
79 Raman scattering compound, availability of large number of Raman labels which have
80 broaden up the scope to select the right label according to the experimental design
81 applications, unique spectral fingerprint from the Raman tag upon laser excitation and the
82 narrow spectrum peak widths that opens up the opportunity of high level multiplex
83 detection (Kneipp et al. 2006; Zhang et al. 2010). SERS phenomenon can be explained by the

84 two enhancement mechanisms, the electromagnetic and the chemical or charge transfer
85 mechanisms. Electromagnetic enhancement is due to the enhanced electromagnetic fields
86 localized to few nanometers of a nanostructured metallic surface formed by surface
87 plasmon resonances while chemical enhancement results from the resonant charge transfer
88 effects between the metal and the molecule that is strongly chemically adsorbed onto its
89 surface (Khalil et al. 2016; Maher 2012). However, nanoparticle-based SERS signaling is
90 mostly dependent on the highly localized regions of intense local field 'hot spots' which is
91 formed in the nanoscale junctions and interstitial crevices of the two or more interacting
92 SERS substrates and consequently provide extraordinary enhancements of up to 10^{15} orders
93 of magnitude to the SERS signal (Hao and Schatz 2004; Qian et al. 2008). Therefore, metallic
94 nanostructures in different forms such as nanoparticles, nanorod, nanogaps, nanoshells,
95 nanostars, dimers, and many more as well as combination of different materials were
96 utilized to explore the hot spots and employed in DNA sensing as it could greatly increase
97 the Raman cross section of the immobilized biomolecules, leading to a low detection limit
98 (Khalil et al. 2016; Lu et al. 2011). GO-AuNP hybrid composites have recently been proved as
99 an effective SERS platforms due to the synergistic effect of two individual components
100 which can magnify the weak Raman signals (Khalil et al. 2016). However, the integration of
101 GO-AuNP hybrid composites with AuNPs has never been explored which we believe can
102 further enhance the Raman signal of the adsorbed molecules with many order of magnitude
103 via electromagnetic and chemical enhancement in comparison to the individual components
104 (either GO, AuNPs or GO-AuNP hybrid alone). **Thus, DNA sensing strategy that uses both GO-
105 AuNP hybrid composite and AuNPs as the sensor platforms, could revolutionize the current
106 biosensing techniques for detecting endangered species as well as DNA biomarkers for
107 many diseases including cancer.**

108 Herein we develop a novel and PCR free SERS DNA biosensor which utilizes a
109 sandwich platform comprising of GO-AuNPs hybrid for target capture and SERS tagged
110 AuNPs for target detection. The hybridization of target sequence with the capture and
111 detection probe facilitates the covalent agglomeration of the strongly coupled plasmonic
112 AuNPs over GO-AuNPs and thereby exhibits locally enhanced electromagnetic field at the
113 junction. The use of dual platforms thus significantly enhanced the SERS signal due to the
114 'hot spot' generation between GO-AuNPs and AuNPs system (Hao and Schatz 2004; He et al.
115 2012; Qian et al. 2008). The developed platform detects target DNA sequence of

116 endangered MBT species, using a short length DNA capture probe which is a limitation for
117 current PCR based techniques. In our study, the Raman tag was attached directly onto the
118 AuNPs surfaces which minimizes the distance dependent limitations, and produced intense
119 SERS spectra by the charge transfer mechanism between the Cy3 and AuNP surfaces
120 (Wabuyele and Vo-Dinh 2005). With this greater amplification of the SERS signal generated
121 by the sandwich duplex structure, a detection limit of as low as 10 fM is achieved.
122 Moreover, our dual platform shows excellent sequence specificity and sensitivity to
123 discriminate single-base mismatches. In comparison with other SERS DNA biosensors, our
124 fabricated sandwich biosensor is cost effective and avoids complex manipulation of ssDNA
125 probe without intercalating the Raman tags. **We believe that this simple but highly selective,
126 specific and sensitive DNA sensing approach would be useful for wide-range of biosensing
127 applications.**
128

1292. **Materials and Methods**

130 **2.1. Chemicals and Instruments**

131 Gold chloride trihydrate ($\text{HAuCl}_4 \cdot 3\text{H}_2\text{O}$), sodium citrate dihydrate ($\text{C}_6\text{H}_5\text{Na}_3\text{O}_7 \cdot 2\text{H}_2\text{O}$) ($\geq 99\%$),
132 graphite powder ($< 20\mu\text{m}$), tris(2-carboxyethyl) phosphine hydrochloride ($\geq 98\%$) (TCEP) and
133 Tris-EDTA (TE) buffer solution, pH 7.4 were obtained from Sigma Aldrich. Potassium
134 permanganate (KMnO_4), phosphoric acid (H_3PO_4) were purchased from R & M Chemicals
135 Ltd.; sulphuric acid (H_2SO_4) (95-97%), hydrochloric acid (HCl) (37%), and ethanol (99.8%)
136 from Friendemann Schmidt and hydrogen peroxide (H_2O_2) (35%) from Quality Reagent
137 Chemical (Qrec). DPEC treated water was purchased from Biobasic Canada Inc. while
138 ultrapure water (UPW) ($18.2 \text{ M}\Omega \text{ cm}$) was prepared from CASCADA LS Water, Pall UltraPure
139 Water System and used throughout the study. The rest of the chemicals were of analytical
140 reagent grade and used as per requirement.

141 Washing and purification of the GO, AuNP and GO-AuNPs were done by using high
142 speed Heraeus Multifuge X3FR Centrifuge, Thermo Scientific. On the contrary, Mini-15K CE
143 High Speed Mini Centrifuge was employed throughout the study for the washing of
144 unbound DNA, washing or separation of nanoparticles/nanocomposites. Ultrasonic
145 homogenizer (TF-650Y) was used for the exfoliation of GO. UV-vis experiments were
146 conducted by using UV-2600 UV-vis spectrophotometer (Shimadzu co., Ltd, Japan). High

147 resolution Transmission electron microscopy (HRTEM) was performed using lacy carbon
 148 coated copper grid with FEI Tecnai F20 TWIN 200kV transmission electron microscope (FEI
 149 company, Hillsboro, USA). X-ray diffraction (XRD) was performed by using PANalytical X-ray
 150 diffractometer (model EMPYREAN, Almelo, Netherlands). SERS spectra were recorded using
 151 Renishaw Invia Confocal Raman Microscope. Atomic Force Microscopy (AFM) was
 152 performed using AFM5000II Scanning Probe Microscope (Hitachi) in dynamic force (tapping)
 153 mode.

154 2.2. Probe, Target and Non-Target DNAs

156 The probe DNA sequence (31-mer) was selected from the short length DNA fragment (120
 157 bp) of mitochondrial cytochrome b (cytb) gene of MBT species. The sequence was
 158 developed and verified by PCR technique for the detection of MBT species from complex
 159 food matrices by Ali, *et al.* (2016) (Ali et al. 2016). As a sensing strategy, the probe DNA
 160 sequence was designed to split into two fractions – 16-mer and 15-mer length which were
 161 further modified with 5' thiol modifier with 6-carbon spacer arm and 3' thiol modifier with
 162 3-carbon spacer arm respectively. All the oligonucleotide sequences (listed in Table 1) were
 163 synthesized and purified by the Integrated DNA Technologies (IDT), Singapore. The
 164 lyophilized oligonucleotides were resuspended in TE buffer (10 mM Tris HCl, 1 mM EDTA, pH
 165 7.4) as per manufacturer instructions and kept at -40°C as stock solution in 100 µM
 166 concentration. To prepare the working standard or dilution from the stock solution, DPEC
 167 treated water was used throughout the study.

168 Table 1: List of oligonucleotide sequences

Name	Sequence profile
Capture probe 1 (16-mer) (CP1)	: SH-(CH ₂) ₆ -5'-GAT-CAT-TAC-TAG-GCA-C 3'
Capture probe 2 (15-mer) (CP2)	: 5'CTG-CCT-AAT-CCT-TCA 3'-(CH ₂) ₃ -SH
Target DNA	: 5'TGA-AGG-ATT-AGG-CAG-GTG-CCT-AGT-AAT-GAT-C3'
Non-complementary DNA	: 5'CAG-GAA-GCC-GAA-TGA-ACA-TTC-GAC-GGC-AGC-T3'
Non-target DNA (Buffalo)	: 5'TGC-AGG-ATT-AGG-CAG-ATG-CCT-AGG-AGA-GAG-C3'
Non-target DNA (Horse)	: 5'TGG-AGG-ATT-AGG-CAG-ATT-CCT-AGG-AGG-GAG-C3'
Non-target DNA (Cow)	: 5'TGT-AGG-ATT-AGG-CAG-ATT-CCC-AGG-AGG-GAA-C3'
Non-target DNA (Pork)	: 5'AGG-GCG-GTA-ATG-ATG-AAT-GGC-AGG3'

Non-target DNA (Dog)	: 5'TGG-CTG-TGT-CCG-ATG-TAT-AGT-GCA-AGT-CCA-CTT3'
One-base mismatch DNA	: 5'TGA-AGG-ATT-AGG-CAA-GTG-CCT-AGT-AAT-GAT-C3'
Three-base mismatch DNA	: 5'TGA-AGG-ATT-AGG-TGA-GTG-CCT-AGT-AAT-GAT-C3'

169

170 **2.3. Synthesis of GO, AuNPs and GO-AuNP nanocomposites**

171 GO and AuNPs were synthesized as per protocol described by Marcano, *et al.* (Marcano et
172 al. 2010) and Liu, J. *et al.* (Liu and Lu 2006) respectively with few modifications and
173 described in details at supporting information (section 1.1 and 1.2). GO-AuNPs composites
174 were synthesized by the citrate reduction of gold (III) salt as per reported procedure with
175 minor modifications (Goncalves et al. 2009). An aqueous suspension of GO (0.5 mg/mL,
176 20mL) was prepared by ultrasonication for 2 h, followed by the addition of syringe filtered
177 100 mL HAuCl₄·3H₂O solution (1 mM). The resultant suspension was then aged for 30 min
178 with continuous stirring to promote the interaction of Au ions with GO surface. The
179 suspension was then heated until 80 °C and 2 mL of C₆H₅Na₃O₇·2H₂O (300 mmol) aqueous
180 solution was added promptly into it. The reaction was continued at 80 °C with stirring for
181 another 4 h. The resulting GO-AuNPs composite was centrifuged at 6000 RPM for 2 h and
182 washed three times with UPW to eliminate the free AuNPs. The final GO-AuNPs
183 nanocomposite was resuspended in UPW and stored in the refrigerator.

184

185 **2.4. Attachment of thiol-modified capture probe DNA to AuNPs and GO-AuNPs**

186 To activate the thiol-modified oligo DNA, 100 µL of 1 mM CP1 and CP2 were treated
187 separately with 10 µL of freshly prepared 10 mM TCEP and incubated at room temperature
188 (RT) for 1 h. Thiol-activated single-stranded (ss) oligonucleotide was then bound to the
189 AuNPs and GO-AuNPs following the procedure developed by Sun *et al.* with little
190 modifications (Sun et al. 2007). As-prepared AuNPs (3 mL) and GO-AuNPs (500 µL)
191 suspension into two different Eppendorf tubes were centrifuged at 8000 RPM for 30 min
192 and the pellets were re-dispersed with 0.1 mM PBS (pH 7.4) to produce final volume 300 µL
193 and 500 µL respectively. TCEP treated CP1 was added into GO-AuNPs while CP2 into AuNPs
194 tube, mixed well with gentle hand shaking and incubated for 16 h at RT in dark
195 environment. After 16 h, 10 mM PBS (pH 7.4) with 0.1% Tween 20 was added to the mixture
196 to result in a solution with a final buffer concentration of 1mM PBS with 0.01% Tween 20
197 and kept standing for 30 min. Next, the salt aging of the DNA functionalized nanoparticles

198 was initiated slowly with 1 M NaCl to reach the final NaCl concentration of 100 mM. NaCl
199 was added gradually at an interval of 1h and the increment rate was such that after first
200 addition of 1 M NaCl it reached to 10 mM. At each NaCl increment, a certain amount of DNA
201 is attached, allowing the AuNPs and GO-AuNPs to survive the next small increment of salt.
202 Moreover, the conformation of DNA is also changed from being parallel to an upright
203 arrangement on the AuNP surface which provides more effective steric stability as well as
204 make easy availability of DNA sequences for further hybridization (Cutler et al. 2012; Zhang
205 et al. 2013). The samples were further allowed to age under the same conditions for another
206 40 h at RT. The aged solution was then centrifuged at 8000 RPM for 20 min and pipetted off
207 the supernatant as much as possible to remove the free DNA. Functionalized nanoparticles
208 were again dispersed in washing buffer (0.1 mM PBS and 100 mM NaCl, pH 7.4) and
209 centrifuged at 8000 RPM for 20 min and the procedure was repeated for 2-3 times. Finally,
210 GO-AuNP immobilized CP1 (GO-AuNP-CP1) precipitates were dispersed in 0.1 mM PBS (pH
211 7.4) and 100 mM NaCl buffer and stored at refrigerator for further use.

212

213 **2.5. Attachment of Cy3-cysteamine to oligo-functionalized AuNPs**

214 Thiolated Cy3 (1000 μ L, 1 μ M) was treated with 100 μ L of freshly prepared 10 mM TCEP and
215 incubated for 1 h at RT. TCEP treated Cy3 was added to the red oily precipitate of AuNP-CP2,
216 obtained from the previous step and allowed to keep for 24 h with frequent manual stirring.
217 The solution was then centrifuged at 8000 RPM for 20 min and the supernatant was
218 discarded. The precipitate was washed with nanopure water by successive centrifugation
219 and redispersion in nanopure water. It has already been established that formation of
220 monolayer of ssDNA after attachment of thiolated DNA onto AuNPs, there were still spaces
221 on AuNPs surface for the subsequent attachment of Raman tags (Sun et al. 2007).

222

223 **2.6. Fabrication of GO-AuNPs DNA Biosensor**

224 GO-AuNP-CP1 (400 μ L) was incubated with corresponding target DNA (100 μ L) for overnight
225 at RT. GO-AuNP-CP1-Target nanocomposite was centrifuged at 8000 RPM for 20 min and
226 washed twice with washing buffer to remove the unhybridized target DNA. The GO-AuNP-
227 CP1-Target nanocomposite was then dispersed into nanopure water for the subsequent
228 hybridization with equal quantity of AuNP-DNA2-Cy3 in the microcentrifuge tube, shaken
229 manually and incubated at RT for overnight to facilitate the hybridization of the CP2 with

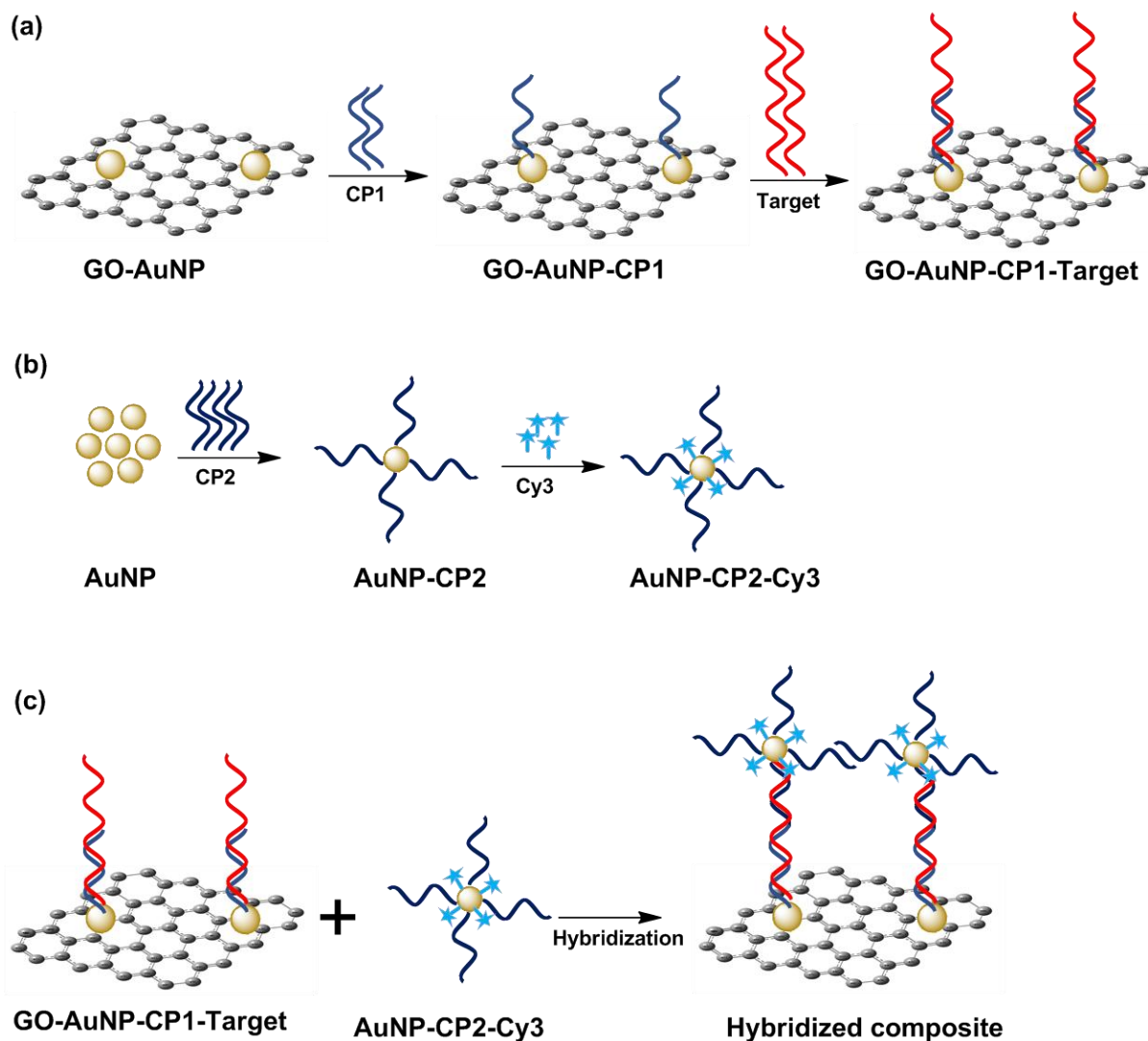
230 the unbound part of the target DNA. The hybridized compound (GO-AuNP-CP1-Target-CP2-
231 AuNP-Cy3) was centrifuged at low speed (4000 RPM for 5 min) and washed several times
232 with washing buffer to remove the unbound AuNP-DNA2-Cy3. The final nanocomposite was
233 dispersed into nanopure water, followed by the preparation of corresponding slide for SERS
234 experiment by dropping 50 μ L each of the sample on the silicon wafer. The sample spot was
235 dried under vacuum created using vacuum pump at ambient condition and SERS spectra
236 were acquired using Renishaw Invia Confocal Raman Microscope with a 20x working
237 objective lens. The sample was excited by using 532 nm laser with 5-mW power at the laser
238 source with 50 μ m diameter spot. All of the obtained Raman spectra were chopped to
239 reveal Raman bands with/without applicable baseline correction. All these manipulations
240 were conducted using the Origin Pro 9.1 software.

241

242 **3. RESULTS AND DISCUSSION**

243 **3.1. Design and principle of the biosensor**

244 The principle of dual platform based (i.e. GO-AuNPs and AuNPs) SERS detection of DNA is
245 illustrated in Fig. 1. We employed a 'sandwich' assay strategy which involves attachment of
246 CP1 on GO-AuNPs composites by the well-established Au-S bonding followed by
247 hybridization with corresponding target sequences (Fig. 1a). On the other hand, CP2 was
248 immobilized onto another platform (i.e. AuNPs) followed by the attachment of Cy3 Raman
249 tag (Fig. 1b). The covalently bound Raman Tags which are in close proximity to the AuNPs
250 surface ensure strong SERS signals to be observed (Sun et al. 2007). CP1 and CP2 are
251 thiolated at the 5' and 3' end respectively which allows facile self-assembly of DNA strands
252 on AuNP surfaces through formation of Au-S bonds (Zhang et al. 2007). In between thiol
253 group and nucleotide bases of the capture probes (CP1 and CP2) we have added 6-carbon
254 spacer to keep the capture probes in upright conformation and free for hybridization as
255 DNA bases in proximity of AuNPs could face difficulties due to steric effect at the surfaces
256 (Park et al. 2002; Zhang et al. 2007). In the construction of SERS biosensor (Fig. 1c), a
257 sandwich complex was formed via a binary networking between the two platforms upon
258 mixing together where CP2 immobilized on AuNPs were hybridized with the remainder
259 target sequence attached to GO-AuNPs (Mucic et al. 1998; Sun et al. 2007). The SERS signal
260 finally confirms the presence of target DNA sequence in the dual platform.



261

262 Fig. 1. The schematic illustration of SERS sandwich biosensor based on GO-AuNPs and AuNPs
 263 dual platforms.

264

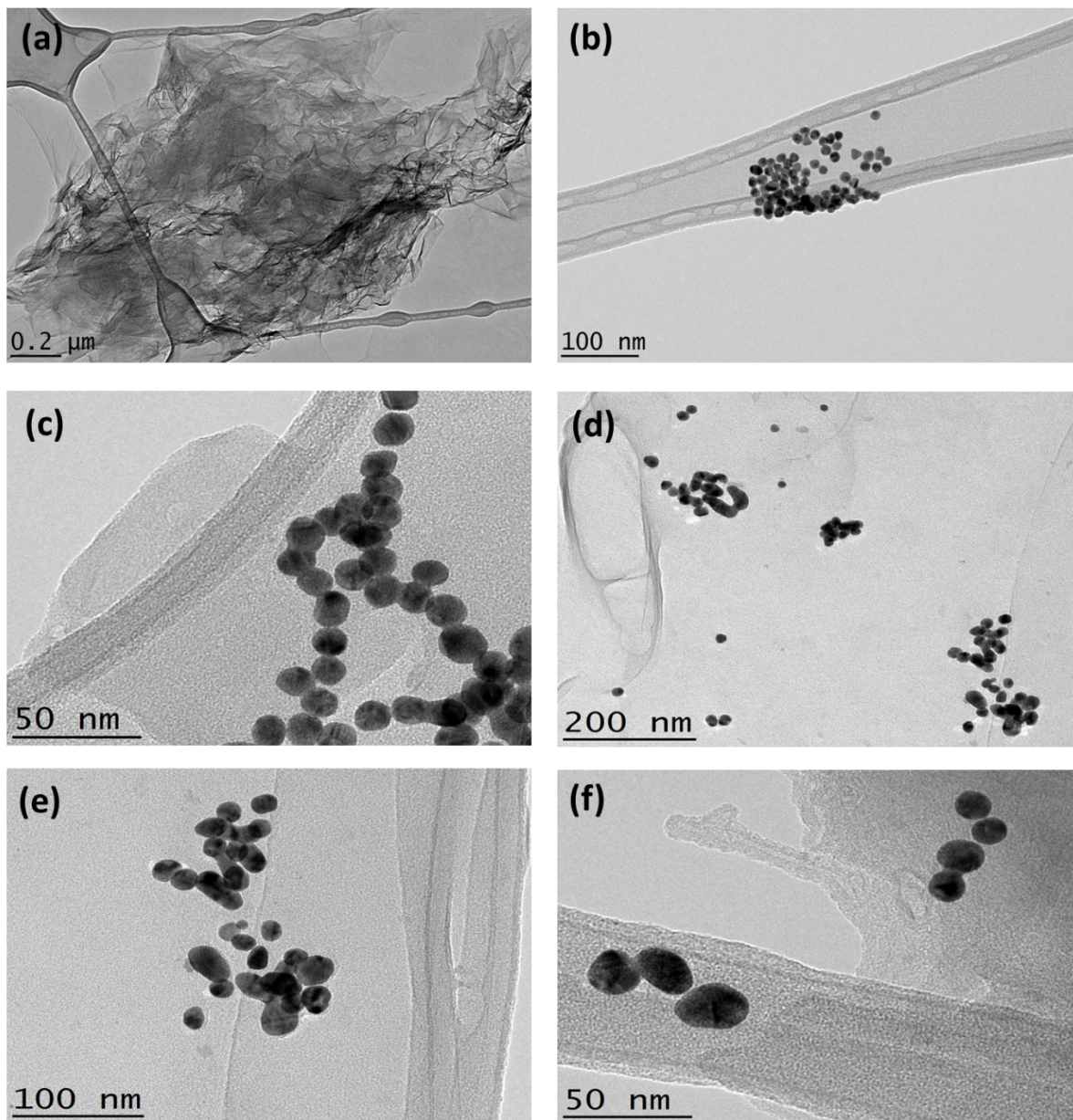
265 3.2. Characterization of GO, AuNPs, and GO-AuNPs nanocomposite

266 The XRD spectra of GO showed a dominant diffraction peak at $2\theta = 10.65^\circ$ corresponding to
 267 an interlayer spacing is 8.30 \AA (Fig. S1a), indicating that the starting graphite flakes had been
 268 oxidized to GO (Marcano et al. 2010). XRD analysis of the synthesized AuNPs represents the
 269 five peaks at $2\theta = 38.19^\circ$ (d-spacing: 2.35 \AA), 44.38° (2.04 \AA), 56.68° (1.62 \AA), 64.70° (1.44 \AA)
 270 and 77.67° (1.22 \AA) (Fig. S1a), corresponding to the Reference code 96-901-1614 of
 271 HighScore Plus library, and standard Bragg reflections (crystal planes) of (111), (200), (200),
 272 (220), and (311) of Au face centers cubic (fcc) lattice. The intense peak at 56.68° represents
 273 the preferential growth in the (200) direction. The GO-AuNP composites also showed the

274 four major peaks at 38.10° (d-spacing: 2.36 Å), 44.30° (2.04 Å), 64.70° (1.44 Å) and 77.64°
275 (1.22 Å) confirming the presence of AuNPs on the GO (Fig. S1a)(Pocklanova et al. 2016).

276 The characteristic UV spectrum of GO exhibited a major peak at 232 nm,
277 corresponding to the plasmonic $\pi \rightarrow \pi^*$ transitions (C=C bonds) (Fig. S1b)(Heuer-Jungemann
278 et al. 2015). The as prepared AuNP solution was burgundy red in color and reflected an
279 absorption band at 520 nm in the visible spectrum (Fig. S1b) (Goncalves et al. 2009). The
280 anticipated shape and diameter of AuNPs are spherical and 13 nm in average which in
281 consequent justified by the HR-TEM examination (Fig. 2b), hence comply the previous study
282 (Liu and Lu 2006). GO-AuNPs hybrids showed two peaks at 240 and 522 nm, representing
283 the characteristic absorption of GO and AuNPs respectively, as well as dictating the
284 successful attachment of AuNPs over GO (Fig. S1b)(Zhang et al. 2012). The result is
285 consistent with HR-TEM (Fig. 2c). The synthesized GO was also characterized by the Raman
286 spectra comprising G-band at 1600 cm^{-1} and D-band at 1350 cm^{-1} whereas GO-AuNP
287 composite was characterized by a moderate blue shift (4 cm^{-1}) as the D-band shifted from
288 1350 cm^{-1} to 1346 cm^{-1} (Fig. S1c). This shift suggests an interaction between AuNPs and GO
289 substrate and ensures AuNPs were deposited on GO (Subrahmanyam et al. 2010). More
290 importantly, there was a significant increase of Raman spectra for GO-AuNPs in compare to
291 GO (~2.5 times higher of G-band value), implies the obvious effect of AuNPs in the
292 synthesized GO-AuNPs which might be due to the electromagnetic SERS enhancement (He
293 et al. 2012; Li et al. 2016).

294



295

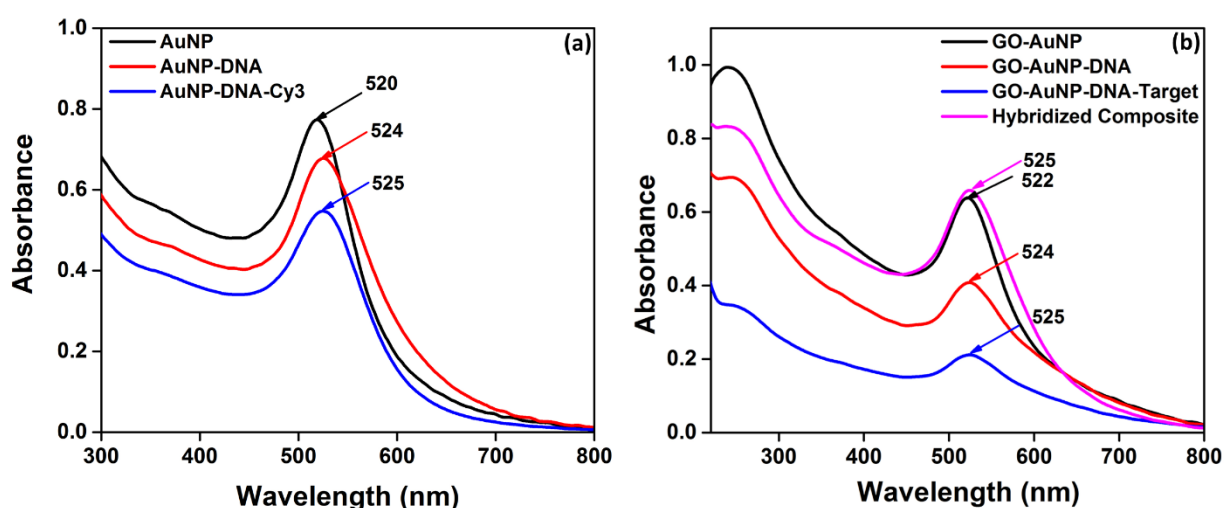
296 Fig. 2. HR-TEM images of (a) GO, (b) AuNP and (c) GO-AuNP on lacy carbon coated copper
 297 grid. (d-f) HR-TEM images of hybridized composites via the coupling of two platforms, GO-
 298 AuNPs and AuNPs via the hybridization of the capture probe sequences with the
 299 complementary target sequence. As hybridization happened, AuNPs were found mostly
 300 aggregated or linked to each other on GO sheets.

301

302 3.3. Attachment of capture probe DNAs and Raman Tag to nanoparticles

303 The conjugation of 15-mer long ssDNA to AuNPs converted the pristine ruby red AuNPs
 304 solution to a pinkish-red solution and this relative reduction of the color density is due to
 305 the reduced amount of free AuNPs (Thavanathan et al. 2014). After the attachment of

306 thiolated DNA on AuNPs, the UV-Vis spectra showed a peak shifting from 520 to 524 nm,
 307 which is due to the increase of AuNPs size through conjugation with DNA probe, suggesting
 308 the successful binding of ssDNA to the AuNPs. Addition of thiolated Cy3 to AuNP-DNA
 309 composite, there was a slight red shifting (1 nm) of the peak at 525 nm, indicating further
 310 increase of the AuNPs size, and confirms the attachment of Cy3 on AuNP-DNA composites
 311 (Fig. 3a) (Thavanathan et al. 2014). Similarly, absorption spectrum of GO-AuNPs hybrids
 312 functionalized with ss-CP1 showed AuNPs characteristic peak shifting from 522 nm to 524
 313 nm (Fig. 3b), confirming the immobilization of thiolated probe DNA over GO-AuNPs (Wang
 314 et al. 2016). However, Atomic Force Microscopy (AFM) study of AuNPs-DNA indicated the
 315 well dispersion of AuNPs (Fig. S2a-d) which may be due to the electrostatic repulsion
 316 between AuNPs for oligo functionalization (Csaki et al. 2001). AFM images of GO-AuNPs
 317 before and after DNA functionalization also justified well distribution of AuNPs on GO sheets
 318 (Fig. Se-h). Moreover, it also demonstrated that AuNPs and GO-AuNPs are stable at gradual
 319 increment of NaCl (1 M) during DNA salt-aging process which thus ensures smooth
 320 hybridization process.



321
 322 Fig. 3. UV-vis absorption spectra of (a) AuNP, AuNPs-ssDNA and AuNP-ssDNA-Cy3 and (b)
 323 GO-AuNPs, GO-AuNPs modified with thiolated CP2, followed by corresponding Target and
 324 finally the hybridized composite.

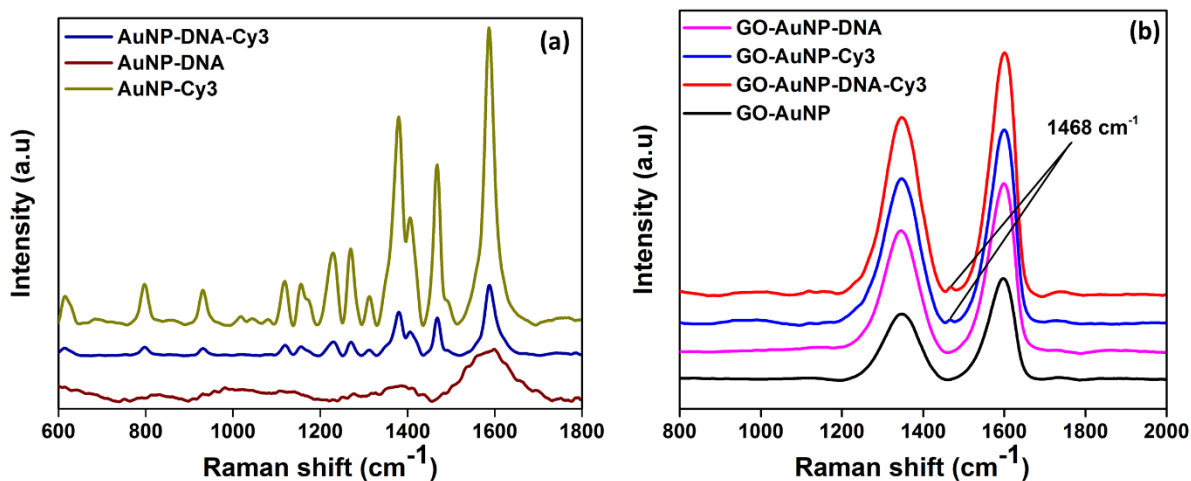
326 3.4. Justification of the Biosensing strategy

327 AuNPs were functionalized with CP2 as well as further modified with thiolated Raman dye
 328 by Au-S linkage and considered as signal probes. Raman spectra of AuNPs-Cy3 reflected the

329 exact fingerprints of Cy3 dye which is characterized by the peaks predominantly at 616, 798,
330 937, 1121, 1158, 1233, 1270, 1384, 1470, and 1592 cm^{-1} (Fig. 4a). Immobilization of Cy3
331 onto AuNPs produced the spectral fingerprint with greater enhancement of Raman
332 scattering which is due to the combined effect of electromagnetic enhancement and charge
333 transfer mechanism (Jans and Huo 2012). However, the incorporation of ss probe DNA to
334 form the composite, AuNPs-CP2-Cy3, had no influence over the Cy3 fingerprint spectra but a
335 decreased intensity. This reduced intensity is proportional to the less immobilized Cy3 which
336 might be due to prior attachment of ss probe DNA to AuNPs (Fig. 4a). Therefore, to
337 demonstrate the feasibility of the signal control, a Cy3 concentration optimization study was
338 conducted and described in the supporting information. The unique features in the signal
339 probe design is that Raman tag was not incorporated in the probe DNA rather directly
340 immobilized onto AuNPs via strong Au-S covalent bonding. Thus avoided complex
341 manipulation in the probe sequences and keeping the ss-probe sequence completely free
342 for hybridization with corresponding target sequences, which made the process robust (Sun
343 et al. 2007).

344 The CP1 was immobilized on SERS active GO-AuNPs nanocomposites by Au-S
345 bonding and used as the detection probes subsequently. Attachment of CP1 onto GO-AuNPs
346 followed by hybridization with corresponding target sequences was confirmed by UV-Vis
347 spectra with broadened red-shifted plasmon band (Fig. 3b) (Storhoff et al. 2000). This
348 widening of the peak might be due to the increasing of the particle size formed by the GO-
349 AuNPs-CP1-Target composite. The hybridization of GO-AuNPs-CP1-Target with CP2-AuNP-
350 Cy3 can be explained by the red shift in the particle surface plasmon resonance from 520 to
351 525 nm, and wide broadening of the peak with greater intensity at 525 nm position which
352 might be due to attachment of more AuNPs composites with the existing GO-AuNPs by the
353 corresponding probe sequences against the target DNA (Fig. 3b) (Mucic et al. 1998; Storhoff
354 et al. 2000). Moreover, to justify the hybridization process by SERS, GO-AuNPs platform was
355 functionalized with Cy3 both in the absence and presence of ss probe DNA. Only a single
356 peak representing the Cy3 at 1468 cm^{-1} is distinguishable and visible as the other major
357 peaks of Cy3 are overlapped by D and G band of GO (Fig. 4b) (Prinz et al. 2016). Therefore,
358 as expected the hybridized composites were also found to produce the SERS peak at 1468
359 cm^{-1} representing the Cy3 attached with AuNPs as well as G-band at 1355 cm^{-1} and D-band

360 at 1590 cm^{-1} characteristic to GO (Fig. S3), ensuring the linking of the two platforms via the
361 covalent attachment of the probes and corresponding target.



362
363 Fig. 4. Raman spectra of AuNPs functionalized with DNA, Cy3 and both DNA and Cy3 (a) GO-
364 AuNP and GO-AuNP functionalized with DNA, Cy3 and both DNA and Cy3 (b).

365 HR-TEM images of the hybridized products also justify that AuNPs are linked with
366 each other in maximum cases which indicates the successful hybridization was happened
367 between the two strands of the CP sequences via complementary target sequences (Fig. 2d-
368 f). However, few single AuNPs also found over the GO sheets, indicating no hybridization
369 happened which might be due to the lack of either strand of the DNA probe sequences or
370 somehow could not find the complementary sequences to be hybridized. Moreover, to
371 justify the hybridization event happened throughout the reaction systems as well as to
372 validate the preparation of the slide for SERS study, a repeatability study of a hybridized
373 composite was conducted by taking SERS spectra from the randomly selected three
374 different locations of the same slide (Fig. S5a). The error of the SERS peak at 1468 cm^{-1} for
375 the three different locations varied only very little with acceptable linearity ($R^2 = 0.94$) (Fig.
376 S5b).

377

378 3.5. Analytical performance of the Biosensor

379 3.5.1. Selectivity of the Biosensor

380 The specificity of the biosensor was solely dependent on the covalent linking of the both
381 platforms via hybridization of split probe sequences with corresponding target DNA and the
382 appearance of representative Cy3 and GO peaks from the SERS spectra. Detection of MBT
383 target sequence is indicated by the presence of D and G band of GO along with peak at 1468

384 cm^{-1} position as Cy3 signatory peak. However, due to the use of short DNA probes in our
385 approach, there is a possibility of having similar nucleotide sequence in the whole genome
386 sequence of other species than MBT. Thus, to check the similarity in sequence, the
387 selectivity of the probe and non-target DNA sequences was justified theoretically. The
388 uniqueness of the 31-mer probe DNA sequence was checked by multiple aligning with cytb
389 gene of MBT and 27 other meat and fish species (Table S1) using MEGA5 alignment tool
390 (<http://www.megasoftware.net/>) which revealed 100% matching only with MBT and scored
391 6-15 nucleotide (19.4-48.4%) mismatching with other non-target species (Table S1),
392 therefore reflecting huge genetic distance and unlikelihood of cross-species recognition in a
393 real experiment. In our experiments, the selectivity of the biosensor was evaluated
394 following different control hybridization reactions accomplished by the presence and
395 absence of target DNA sequences and the replacement of target sequence with non-
396 complementary DNA sequences. In detail, substitution of the target sequence was done by
397 i) 31-mer long oligonucleotide sequence with 100% mismatch nucleotide bases, ii)
398 complementary target sequence of the three non-target species (buffalo, horse and cow)
399 having the 6-8 mismatches (Table S1), and iii) two other non-target sequences with distinct
400 length – pork (24-mer) and dog (33-mer). In the presence of the corresponding target
401 sequence, GO-AuNP-CP1-Target-CP2-AuNP-Cy3 sandwich composite was formed by the
402 coupling of the two platforms, generates the SERS hot spot and consequently strong SERS
403 signal characterized by Cy3 fingerprint peak at 1468 cm^{-1} along with GO representing G and
404 D band (Fig. 5a). This SERS spectra therefore indicates a true positive result (Chuong et al.
405 2017). On the other hand, SERS spectra from the control samples such as hybridized
406 composite with no target sequence (blank sample) generated only GO representing peaks
407 without any existence of Cy3 spectral fingerprint (Fig. 5a), therefore, suggesting no
408 hybridization event due to lack of bridging target sequences. Therefore, the peak intensity
409 at 1468 cm^{-1} for the blank sample is being considered as the baseline signal for Cy3 and the
410 obtained spectra is denoted as the true negative.

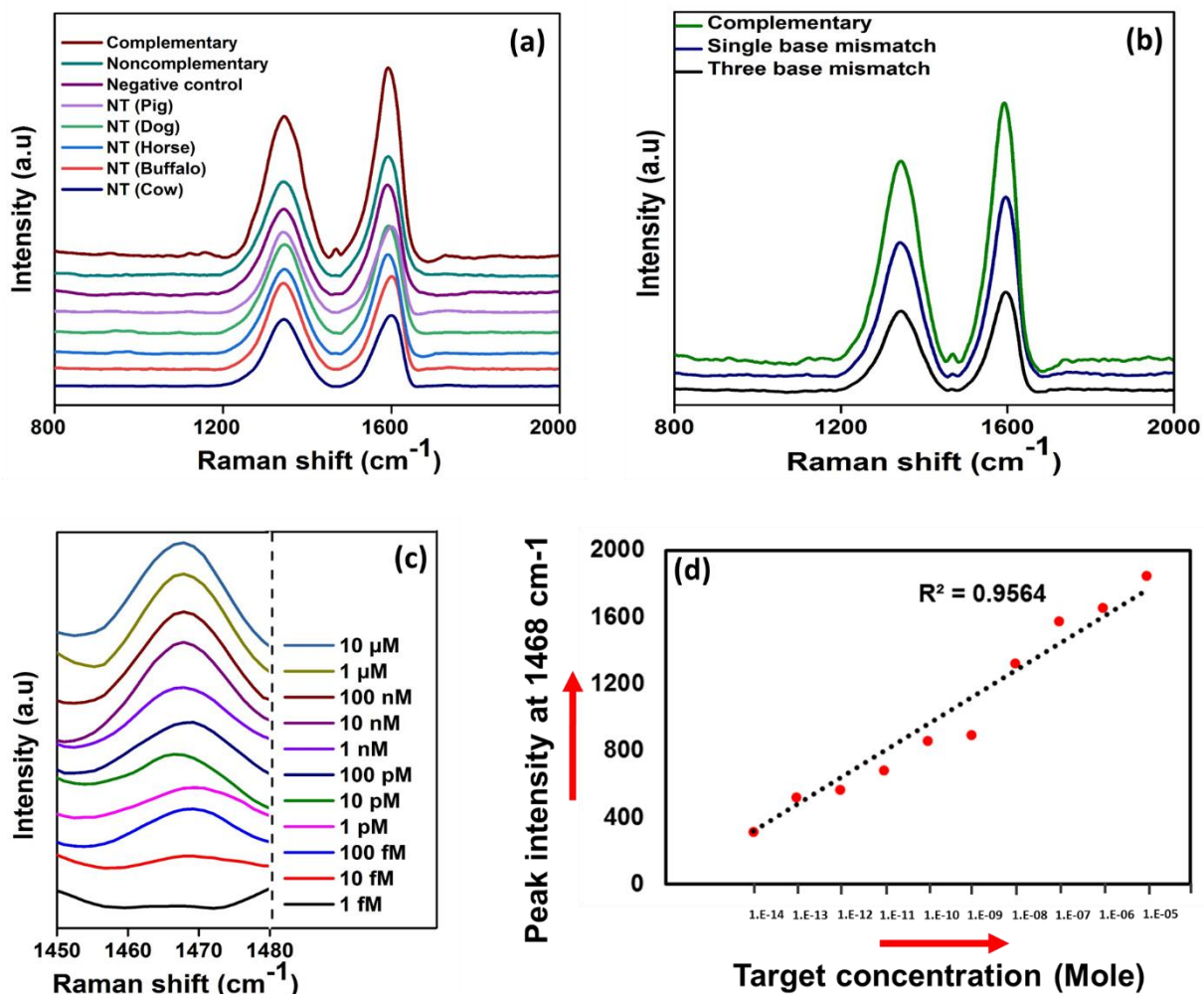
411 The SERS spectra of the hybridized composite achieved in the presence of non-
412 complementary (100% mismatch) and complementary target sequences of the non-target
413 species (cow, buffalo, horse, dog and pig) however, revealed representing GO peaks and in
414 rare cases with very little existence of Cy3 signal (Fig. 5a). The presence of this very weak
415 Cy3 signal could be considered as false positive, and the intensity is ignored in this study due

416 to the equal or lower signal-to-noise ratio. This little existence of Cy3 spectra might be due
417 to some nonspecific interaction between the fabricated GO-AuNPs-CP1-T and AuNPs-CP2-
418 Cy3 composites, however could not produce intense Cy3 SERS signal due to lack of hot-spot
419 generation. This is because hot spots are generally originated at the interstices between
420 adjacent AuNPs rather than between GO sheet and AuNPs (Chuong et al. 2017). Moreover,
421 due to the dominant presence of the D and G band of GO, all other less intense Cy3 peaks
422 were also minimized (Prinz et al. 2016). A true positive signal is therefore distinguishable
423 from the false positive by the distinct Cy3 fingerprint peak at 1468 cm^{-1} . Therefore, the
424 results showed that the fabricated sensor is highly efficient to distinguish target and non-
425 target DNA sequences of the closely related species and suggesting no hybridization event
426 between the capture probes and complementary target sequence of the non-target species.
427 The selectivity experiment thus confirms the theoretical finding that the probe is highly
428 specific for MBT species only and there is no chance for the hybridization with non-target
429 species.

430

431 **3.5.2. Sensitivity of the Biosensor**

432 The efficiency of biosensor in terms of the ability to distinguish the corresponding target
433 sequences bearing single-base mismatch and three-base mismatches were tested. As shown
434 in Fig. 5b, the hybridized composite via the base-mismatch target sequence generated SERS
435 spectra (i.e. Cy3 representative peak at 1468 cm^{-1}) at lower intensity in comparison to the
436 fully complementary sequence. This is attributed to the fact that mismatched DNA might
437 undergo irregular attachment with the complementary probe sequences due to the base
438 changes in the sequence. The data in Fig. 5b thus indicates that the higher the number of
439 base mismatches in the sequence, the lower the SERS intensity due to the irregular
440 hybridization. This data clearly suggests that the developed biosensor is sensitive enough to
441 distinguish the DNA with single nucleotide variation. We believe that one of the main
442 reasons behind this greater efficiency is probably the use of very short fragment of ss DNA
443 (only 15 and 16 bases long) as the probe sequences for detecting target DNA.



444

445 Fig. 5. (a) SERS spectra of the selectivity study. DNA hybridization containing
 446 complementary, non-complementary, negative control (blank) and non-Target sequences
 447 (pig, dog, horse, buffalo, and cow), and (b) SERS spectra of the biosensor hybridized with
 448 corresponding (red), single-base mismatch (dark blue) and three-base mismatches (black)
 449 target sequences. (c) Stacked SERS spectra of Cy3 peak at 1468 cm^{-1} of the composites
 450 hybridized with varying concentration of MBT target DNAs (10 μM to 1 fM), displayed from
 451 the upper to the lower direction. Here, the spectra were chopped into 1450 to 1480 cm^{-1} to
 452 magnify and distinguish the intensity at peak 1468 cm^{-1} . (d) Linear plot of SERS intensities of
 453 1468 cm^{-1} band versus corresponding target DNA concentration.

454

455 3.5.3. Dynamic detection range of the Biosensor

456 Quantitative detection of the target sequence was performed by measuring the SERS
 457 intensity of the representative signal probe - Cy3 from the hybridized compounds formed
 458 via the varying concentration of target DNA. Each Target sample is ten times diluted from its

459 previous concentration to provide a series of target DNA concentration from 10 μM to 1 fM.
460 The SERS intensity was in downward trend with the decreasing concentration of the target
461 DNA from 10 μM to 10 fM (Fig. S6 and Fig. 5c). However, there was no/almost
462 indistinguishable Cy3 signal from the hybridized composite for the target concentration
463 below 10 fM. The SERS spectra were background (baseline) corrected, and a standard curve
464 for the intensity of the Cy3 peak at 1468 cm^{-1} position versus target concentrations was
465 plotted (Fig. 5d). An R^2 value of 0.96 was obtained from the linear regression analysis of the
466 peak height at 1468 cm^{-1} against the corresponding target DNA concentration. This data
467 suggests that our biosensor can be applicable in detecting target DNA sequence from a wide
468 range of sample concentration. This greater sensitivity of our fabricated biosensor relied on
469 few aspects such as using GO-AuNPs as the SERS platform where maximum number of
470 AuNPs were being deposited over the large planer surface of GO which in consequent
471 facilitated the covalent binding of CP1 sequences in greater numbers, hence creating more
472 options even for the minute quantity of the target sequences to be hybridized. Even if single
473 CP2 bound to AuNP-Cy3 hybridize with the corresponding unbound portion of target
474 sequence, the Cy3 signal would be strong due to more Cy3 molecules bound over the same
475 AuNP-CP2 composite (Fig. 1c). Moreover, covalent linking of the detection and signal probe
476 via hybridization event brings the two platforms within few nanometer ranges, therefore
477 generates hotspots at the junction of GO-AuNPs and AuNPs which in consequent lead to
478 strong highly localized enhancement of SERS signal. In addition to the electromagnetic, a
479 minor enhancement due to the resonant charge transfer process between the AuNPs and
480 Cy3 is also contributed to the detected Raman signal. This chemical enhancement might be
481 due to the vibrationally excited state of the adsorbed Cy3 molecule which is caused by two
482 ways - either by exciting electrons from AuNPs to unoccupied molecular orbitals of adsorbed
483 Cy3 and back to the AuNPs or electrons from the occupied molecular orbitals into the Fermi
484 level of AuNPs and back to the adsorbed molecule (Maher 2012; Radziuk and Moehwald
485 2015). Hence to justify the contribution of the hot spots in signal enhancement, SERS
486 spectra of hybridized sandwich composite in absence of Cy3 was compared to bare GO-
487 AuNPs and the enhancement is about 26% more intense than GO-AuNPs (Fig. S7). This
488 enhancement is definitely due to the agglomeration of AuNPs over GO-AuNPs via
489 hybridization and hot spot generated at the junctions between AuNPs rather than AuNPs
490 deposition over GO sheet (Chuong et al. 2017). Moreover, functionalization of AuNPs-CP2

491 with Cy3, followed by hybridization and coupling with GO-AuNPs-CP1-T, enhances SERS
492 signals 15% (Fig. S7) more than the hybridized composite without Cy3, therefore, dictates
493 the contribution of chemical enhancement by the adsorbed Cy3 molecule.

494 The use of SERS active dual nanoparticle platforms, and short length oligo marker,
495 made our biosensor viable and amenable for the detection of trace amount of DNA (e.g.
496 LOD is 10 fM) present in the sample. The fabricated biosensor showed better capability to
497 detect MBT species in comparison to the some of the PCR based detection techniques
498 involving 120 base pair long amplicon by conventional PCR, PCR-RFLP and SYBR green real-
499 time PCR techniques (Ali et al. 2015; Ali et al. 2016; Asing et al. 2016). Hence, the detection
500 principle will be efficient enough for the unambiguous tracing of MBT materials in the food
501 chain, or any forensic or archaeological investigations and tracking of trafficking. Moreover,
502 SERS biosensors exhibited better sensitivity than the biosensors fabricated by single
503 platform using Raman label at the terminal end of reporter DNA (He et al. 2012) and even
504 using the dual platforms following sandwich assay procedure (Kang et al. 2010; Zhang et al.
505 2010). Some of the sandwich assay procedure involved SERS non-active platform hence
506 required further step such as exfoliation of a graphene layer over the hybridized composite
507 (Prinz et al. 2016) or silver enhancement of the hybridized composites (Cao et al. 2002).
508 Therefore, to address the shortcomings as well as to make the sensing way easy, flawless,
509 and convenient, we have employed two different SERS active platforms and only few simple
510 steps involvement to produce multi-component aggregates upon hybridization to get
511 greater SERS intensity via the localized hot spots. Furthermore, Cy3 was directly immobilized
512 onto the AuNPs which also directly contributed on the total enhancement by the charge
513 transfer mechanisms. Finally, we believe that using different SERS active substrate and
514 applying the same biosensing principle, it will be possible to establish a multiplex DNA
515 sensor for the detection of multiple DNA biomarker sequences from different origin.

516

517 **4. Conclusion**

518 We have demonstrated dual platform-based PCR free SERS assay for the efficient and
519 sensitive detection of DNA. To fabricate the device, short probe sequences were
520 immobilized onto two different nanostructure platforms to form GO-AuNPs-CP1 and AuNPs-
521 CP2-Cy3, considered as detection and signal probe respectively. The novel features of the
522 sensor are the use of very short length probe sequences and the linking of the two SERS

523 active platforms via target-probe DNA hybridization to produce a unique and enhanced SERS
524 signal. This huge enhancement is in fact due to the combined effects of electromagnetic
525 enhancement via the hot spot generated by multicomponent assembly as well as the
526 chemical enhancement by the charge transfer mechanism between Cy3 and AuNPs surfaces.
527 Therefore, the presence of target DNA up to 10 fM, was even able to combine the two
528 platforms together to generate the unique and distinguishable SERS spectra. The biosensors
529 thus provide the LOD down to 10 fM and could differentiate the target sequences difference
530 with single nucleotide variation. Furthermore, the fabrication of the biosensor is easy,
531 convenient, involves low-cost SERS substrate and provides extraordinary specificity to
532 discriminate the corresponding sequences of the closely related non-target meat species.
533 The SERS biosensor thus revealed better suitability and efficiency for the detection and
534 quantification of MBT materials in the food chain to remove the ambiguity, hence could be
535 adopted by the regulatory authorities, archaeologists and wildlife protection agencies for
536 the forensic or archaeological authentication even under compromised conditions as well as
537 tracking of the MBT trafficking with greater reliability and confidence. Moreover, this PCR
538 free, short length split-probe DNA conjugated dual platforms based SERS sensing technology
539 will also be suitable for detecting any short length DNA biomarkers. Thus, we believe that
540 this platform could be considered as a model for the detection of life threatening
541 pathogenic microorganisms, cancers, verification of food adulteration, authentication of
542 species, forensic applications and guided us for the multiplex detection.

543

544 **Acknowledgement**

545 The authors would like to thank Dr. Equb Ali and Dr. M.A. Motalib Hossain, University of
546 Malaya for their intellectual support and assistance in providing Lab facility for oligo DNA
547 handling and storage. This work was financially supported by the Grand Challenge project
548 (GC001B-14SBS), Postgraduate Research Grant (PPP) (PG190-2015B) and UMRG programme
549 (RP044C-17AET) of University of Malaya, Malaysia.

550

551 **References**

552 Ali, M.E., Asing, Hamid, S.B.A., Razzak, M.A., Rashid, N.R.A., Al Amin, M., Mustafa, S., 2015. A
553 suitable method to detect potential fraud of bringing Malayan box turtle (Cuora

554 amboinensis) meat into the food chain. *Food Additives & Contaminants: Part A* 32(8), 1223-
555 1233.

556 Ali, M.E., Hamid, S.B.A., Hossain, M.M., Mustafa, S., Kader, M.A., Zaidul, I., 2016. Lab-on-a-
557 chip-based PCR-RFLP assay for the detection of malayan box turtle (*Cuora amboinensis*) in
558 the food chain and traditional Chinese medicines. *PLoS one* 11(10), e0163436.

559 Ali, M.E., Kashif, M., Uddin, K., Hashim, U., Mustafa, S., Man, Y.B.C., 2012. Species
560 authentication methods in foods and feeds: the present, past, and future of halal forensics.
561 *Food Analytical Methods* 5(5), 935-955.

562 Asing, Ali, E., Hamid, S.B.A., Hossain, M., Ahamad, M.N.U., Hossain, S.A., Naquiah, N., Zaidul,
563 I., 2016. Duplex real-time PCR assay using SYBR Green to detect and quantify Malayan box
564 turtle (*Cuora amboinensis*) materials in meatballs, burgers, frankfurters and traditional
565 Chinese herbal jelly powder. *Food Additives & Contaminants: Part A* 33(11), 1643-1659.

566 Cao, Y.C., Jin, R., Mirkin, C.A., 2002. Nanoparticles with Raman spectroscopic fingerprints for
567 DNA and RNA detection. *Science* 297(5586), 1536-1540.

568 Chuong, T.T., Pallaoro, A., Chaves, C.A., Li, Z., Lee, J., Eisenstein, M., Stucky, G.D., Moskovits,
569 M., Soh, H.T., 2017. Dual-reporter SERS-based biomolecular assay with reduced false-
570 positive signals. *Proceedings of the National Academy of Sciences* 114(34), 9056-9061.

571 Csaki, A., Möller, R., Straube, W., Köhler, J., Fritzsche, W.J.N.A.R., 2001. DNA monolayer on
572 gold substrates characterized by nanoparticle labeling and scanning force microscopy
573 29(16), e81-e81.

574 Cutler, J.I., Auyeung, E., Mirkin, C.A., 2012. Spherical nucleic acids. *Journal of the American*
575 *Chemical Society* 134(3), 1376-1391.

576 Goncalves, G., Marques, P.A., Granadeiro, C.M., Nogueira, H.I., Singh, M., Gracio, J., 2009.
577 Surface modification of graphene nanosheets with gold nanoparticles: the role of oxygen
578 moieties at graphene surface on gold nucleation and growth. *Chemistry of Materials* 21(20),
579 4796-4802.

580 Green, A.D., Buhlmann, K.A., Hagen, C., Romanek, C., Gibbons, J.W.J.J.o.e.h., 2010. Mercury
581 contamination in turtles and implications for human health 72(10), 14-23.

582 Ha, N.-R., Jung, I.-P., La, I.-J., Jung, H.-S., Yoon, M.-Y., 2017. Ultra-sensitive detection of
583 kanamycin for food safety using a reduced graphene oxide-based fluorescent aptasensor.
584 *Scientific reports* 7, 40305.

585 Hao, E., Schatz, G.C., 2004. Electromagnetic fields around silver nanoparticles and dimers.
586 *The Journal of chemical physics* 120(1), 357-366.

587 He, S., Liu, K.-K., Su, S., Yan, J., Mao, X., Wang, D., He, Y., Li, L.-J., Song, S., Fan, C., 2012.
588 Graphene-based high-efficiency surface-enhanced Raman scattering-active platform for
589 sensitive and multiplex DNA detection. *Analytical chemistry* 84(10), 4622-4627.

590 Heuer-Jungemann, A., Kiessling, L., Stratakis, E., Kymakis, E., El-Sagheer, A.H., Brown, T.,
591 Kanaras, A.G., 2015. Programming the assembly of gold nanoparticles on graphene oxide
592 sheets using DNA. *Journal of Materials Chemistry C* 3(36), 9379-9384.

593 Hird, H., Chisholm, J., Sánchez, A., Hernandez, M., Goodier, R., Schneede, K., Boltz, C.,
594 Popping, B., 2006. Effect of heat and pressure processing on DNA fragmentation and
595 implications for the detection of meat using a real-time polymerase chain reaction. *Food*
596 *additives and contaminants* 23(7), 645-650.

597 Huang, R., He, N., Li, Z., 2018. Recent progresses in DNA nanostructure-based biosensors for
598 detection of tumor markers. *Biosensors and Bioelectronics* 109, 27-34.

599 Jans, H., Huo, Q., 2012. Gold nanoparticle-enabled biological and chemical detection and
600 analysis. *Chemical Society Reviews* 41(7), 2849-2866.

601 Kang, T., Yoo, S.M., Yoon, I., Lee, S.Y., Kim, B., 2010. Patterned multiplex pathogen DNA
602 detection by Au particle-on-wire SERS sensor. *Nano letters* 10(4), 1189-1193.

603 Khalil, I., Julkapli, N.M., Yehye, W.A., Basirun, W.J., Bhargava, S.K., 2016. Graphene–Gold
604 Nanoparticles Hybrid—Synthesis, Functionalization, and Application in a Electrochemical
605 and Surface-Enhanced Raman Scattering Biosensor. *Materials* 9(6), 406.

606 Kneipp, K., Kneipp, H., Bohr, H.G., 2006. Single-molecule SERS spectroscopy. *Surface-*
607 *Enhanced Raman Scattering*, pp. 261-277. Springer.

608 Li, Y., Cu, Y.T.H., Luo, D., 2005. Multiplexed detection of pathogen DNA with DNA-based
609 fluorescence nanobarcodes. *Nature biotechnology* 23(7), 885-889.

610 Li, Y., Yang, J., Zhou, Y.-z., Zhong, T., Zheng, S.-h., Zeng, W.-w., 2016. Facile synthesis of gold
611 nanoparticles-graphene oxide films and their excellent surface-enhanced Raman scattering
612 activity. *Monatshefte für Chemie-Chemical Monthly* 147(4), 677-683.

613 Liu, J., Lu, Y., 2006. Preparation of aptamer-linked gold nanoparticle purple aggregates for
614 colorimetric sensing of analytes. *Nature protocols* 1(1), 246.

615 Lu, G., Li, H., Liusman, C., Yin, Z., Wu, S., Zhang, H., 2011. Surface enhanced Raman
616 scattering of Ag or Au nanoparticle-decorated reduced graphene oxide for detection of
617 aromatic molecules. *Chemical Science* 2(9), 1817-1821.

618 Maher, R.C., 2012. SERS Hot Spots. In: Kumar, C.S.S.R. (Ed.), *Raman Spectroscopy for*
619 *Nanomaterials Characterization*, pp. 215-260. Springer Berlin Heidelberg, Berlin, Heidelberg.

620 Marcano, D.C., Kosynkin, D.V., Berlin, J.M., Sinitskii, A., Sun, Z., Slesarev, A., Alemany, L.B.,
621 Lu, W., Tour, J.M., 2010. Improved Synthesis of Graphene Oxide. *ACS Nano* 4(8), 4806-4814.

622 Merkoçi, A., 2010. Nanoparticles-based strategies for DNA, protein and cell sensors.
623 *Biosensors and Bioelectronics* 26(4), 1164-1177.

624 Mucic, R.C., Storhoff, J.J., Mirkin, C.A., Letsinger, R.L., 1998. DNA-Directed Synthesis of
625 Binary Nanoparticle Network Materials. *Journal of the American Chemical Society* 120(48),
626 12674-12675.

627 Ngo, H.T., Wang, H.-N., Fales, A.M., Vo-Dinh, T., 2016. Plasmonic SERS biosensing nanochips
628 for DNA detection. *Analytical and bioanalytical chemistry* 408(7), 1773-1781.

629 Nie, S., Emory, S.R., 1997. Probing single molecules and single nanoparticles by surface-
630 enhanced Raman scattering. *Science* 275(5303), 1102-1106.

631 Park, S.-J., Taton, T.A., Mirkin, C.A., 2002. Array-based electrical detection of DNA with
632 nanoparticle probes. *Science* 295(5559), 1503-1506.

633 Pocklanova, R., Rath, A.K., Gawande, M.B., Datta, K.K.R., Ranc, V., Cepe, K., Petr, M., Varma,
634 R.S., Kvitek, L., Zboril, R., 2016. Gold nanoparticle-decorated graphene oxide: Synthesis and
635 application in oxidation reactions under benign conditions. *Journal of Molecular Catalysis A:*
636 *Chemical* 424, 121-127.

637 Prinz, J., Matković, A., Pešić, J., Gajić, R., Bald, I., 2016. Hybrid Structures for
638 Surface-Enhanced Raman Scattering: DNA Origami/Gold Nanoparticle Dimer/Graphene.
639 *Small* 12(39), 5458-5467.

640 Qian, X., Zhou, X., Nie, S., 2008. Surface-enhanced Raman nanoparticle beacons based on
641 bioconjugated gold nanocrystals and long range plasmonic coupling. *Journal of the*
642 *American Chemical Society* 130(45), 14934-14935.

643 Radziuk, D., Moehwald, H., 2015. Prospects for plasmonic hot spots in single molecule SERS
644 towards the chemical imaging of live cells. *Physical Chemistry Chemical Physics* 17(33),
645 21072-21093.

646 Saidur, M.R., Aziz, A.R.A., Basirun, W.J., 2017. Recent advances in DNA-based
647 electrochemical biosensors for heavy metal ion detection: A review. *Biosensors and*
648 *Bioelectronics* 90, 125-139.

649 Shahrokhian, S., Salimian, R., 2018. Ultrasensitive detection of cancer biomarkers using
650 conducting polymer/electrochemically reduced graphene oxide-based biosensor:
651 Application toward BRCA1 sensing. *Sensors and Actuators B: Chemical* 266, 160-169.

652 Storhoff, J.J., Lazarides, A.A., Mucic, R.C., Mirkin, C.A., Letsinger, R.L., Schatz, G.C., 2000.
653 What Controls the Optical Properties of DNA-Linked Gold Nanoparticle Assemblies? *Journal*
654 *of the American Chemical Society* 122(19), 4640-4650.

655 Subrahmanyam, K.S., Manna, A.K., Pati, S.K., Rao, C.N.R., 2010. A study of graphene
656 decorated with metal nanoparticles. *Chemical Physics Letters* 497(1), 70-75.

657 Sun, L., Yu, C., Irudayaraj, J., 2007. Surface-enhanced Raman scattering based
658 nonfluorescent probe for multiplex DNA detection. *Analytical chemistry* 79(11), 3981-3988.

659 Thavanathan, J., Huang, N.M., Thong, K.L., 2014. Colorimetric detection of DNA
660 hybridization based on a dual platform of gold nanoparticles and graphene oxide.
661 *Biosensors and Bioelectronics* 55, 91-98.

662 Tondro, G., Vais, R.D., Sattarahmady, N., 2018. An optical genosensor for *Enterococcus*
663 *faecalis* using conjugated gold nanoparticles-rRNA oligonucleotide. *Sensors and Actuators B:*
664 *Chemical* 263, 36-42.

665 Turna, J., Marcela, B., Domenico, P., 2010. Polymerase chain reaction–restriction fragment
666 length polymorphism (PCR-RFLP) as a molecular discrimination tool for raw and heat-
667 treated game and domestic animal meats. *Journal of Food and Nutrition Research* 49(3),
668 134-139.

669 Wabuyele, M.B., Vo-Dinh, T., 2005. Detection of human immunodeficiency virus type 1 DNA
670 sequence using plasmonics nanoprobe. *Analytical chemistry* 77(23), 7810-7815.

671 Wang, Q., Li, Q., Yang, X., Wang, K., Du, S., Zhang, H., Nie, Y., 2016. Graphene oxide–gold
672 nanoparticles hybrids-based surface plasmon resonance for sensitive detection of
673 microRNA. *Biosensors and Bioelectronics* 77, 1001-1007.

674 Xu, L.-J., Lei, Z.-C., Li, J., Zong, C., Yang, C.J., Ren, B., 2015. Label-free surface-enhanced
675 Raman spectroscopy detection of DNA with single-base sensitivity. *Journal of the American*
676 *Chemical Society* 137(15), 5149-5154.

677 Zhang, H., Harpster, M.H., Park, H.J., Johnson, P.A., Wilson, W.C., 2010. Surface-enhanced
678 Raman scattering detection of DNA derived from the West Nile virus genome using
679 magnetic capture of Raman-active gold nanoparticles. *Analytical chemistry* 83(1), 254-260.

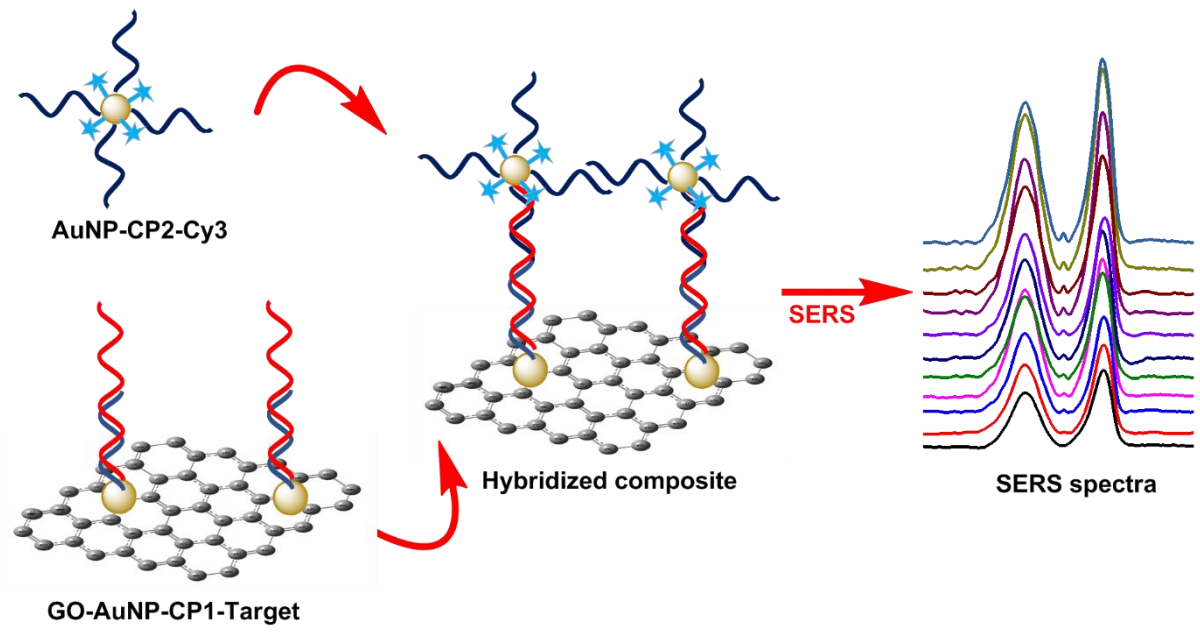
680 Zhang, J., Song, S., Wang, L., Pan, D., Fan, C., 2007. A gold nanoparticle-based
681 chronocoulometric DNA sensor for amplified detection of DNA. *Nature protocols* 2(11),
682 2888-2895.

683 Zhang, Q., Ren, Q., Miao, Y., Yuan, J., Wang, K., Li, F., Han, D., Niu, L., 2012. One-step
684 synthesis of graphene/polyallylamine–Au nanocomposites and their electrocatalysis toward
685 oxygen reduction. *Talanta* 89, 391-395.

686 Zhang, X., Gouriye, T., Göeken, K., Servos, M.R., Gill, R., Liu, J., 2013. Toward fast and
687 quantitative modification of large gold nanoparticles by thiolated DNA: scaling of nanoscale
688 forces, kinetics, and the need for thiol reduction. *The Journal of Physical Chemistry C*
689 117(30), 15677-15684.

690

Graphical Abstract



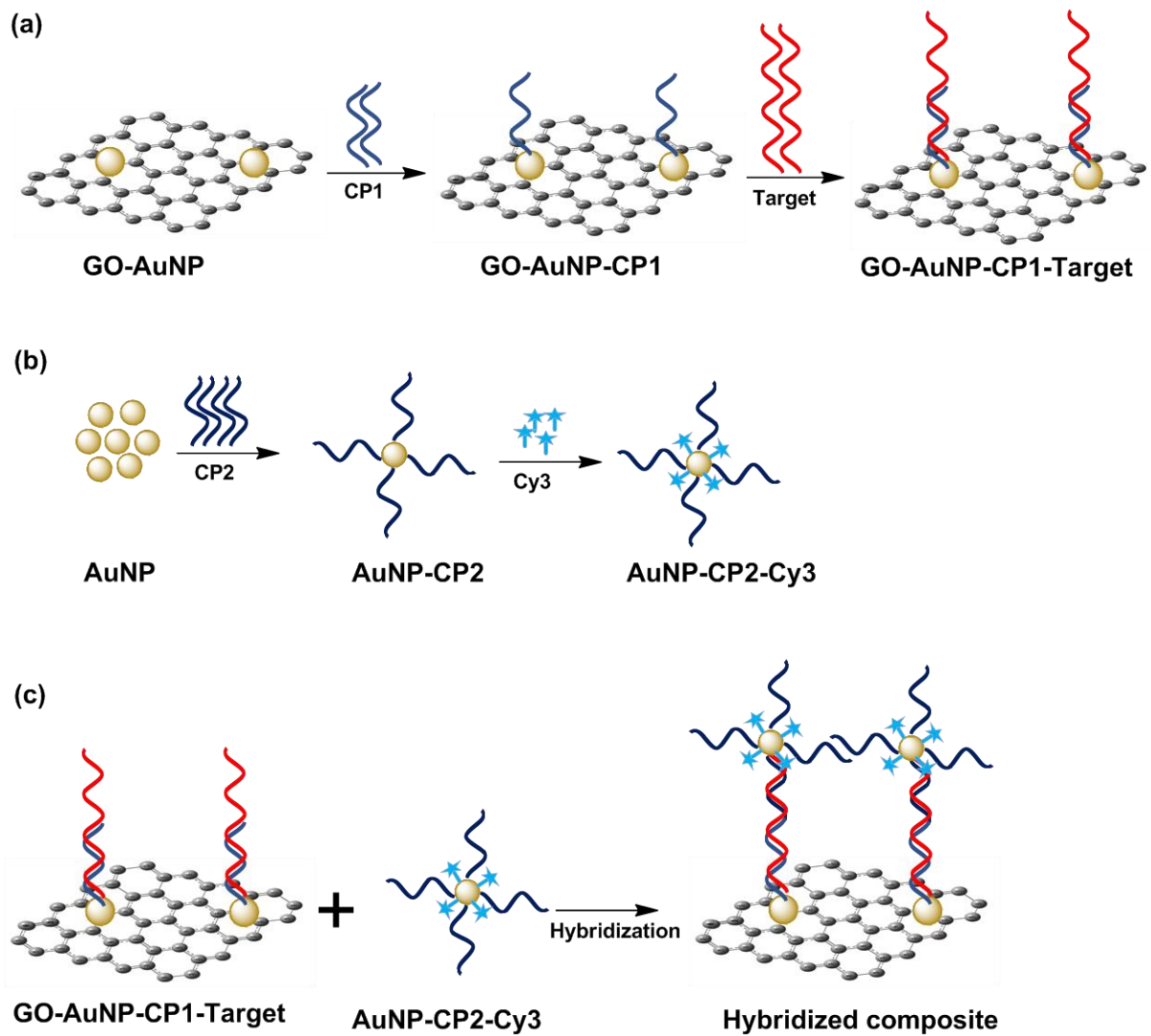


Fig. 1. The schematic illustration of SERS sandwich biosensor based on GO-AuNPs and AuNPs dual platforms.

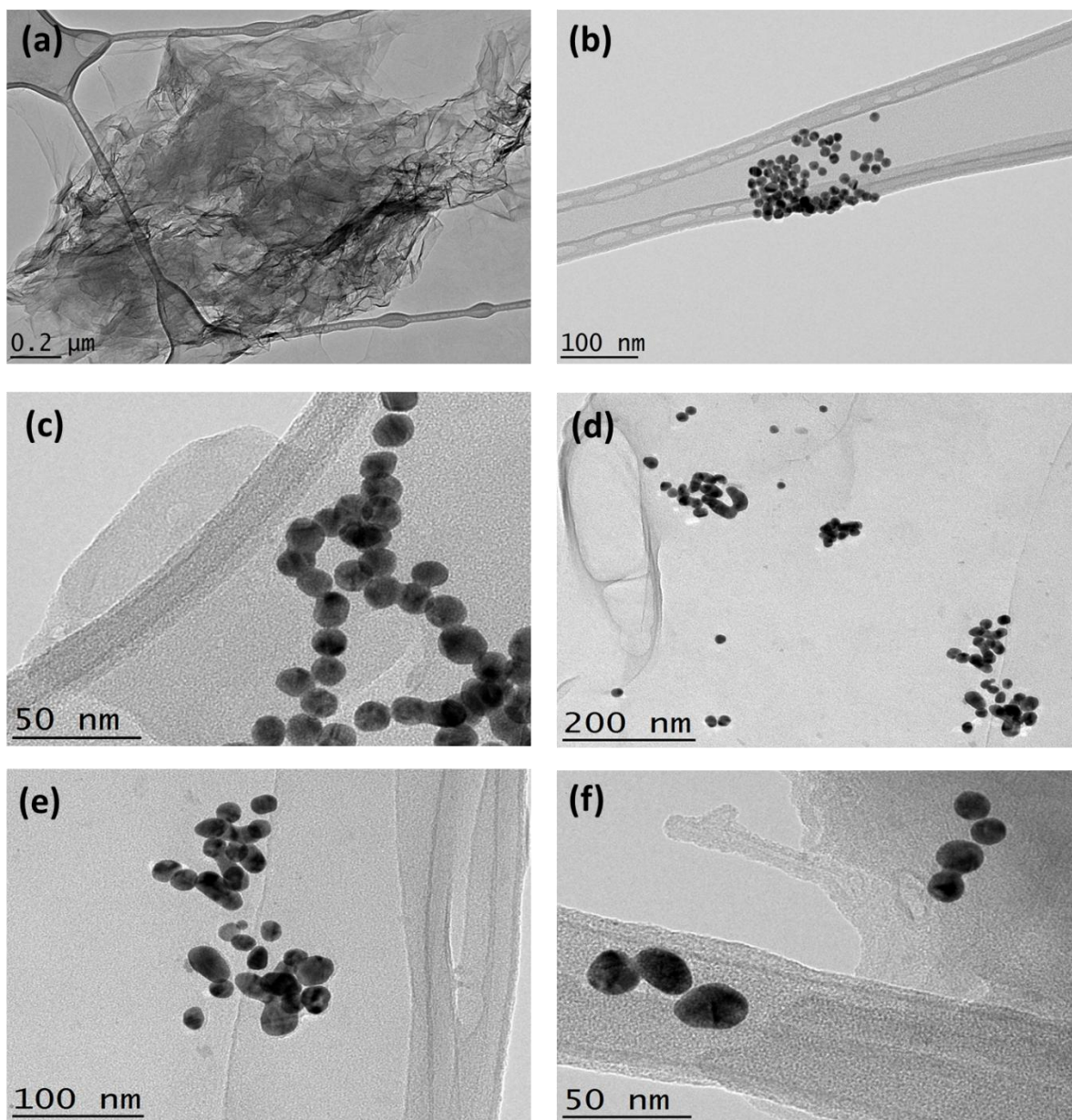


Fig. 2. HR-TEM images of (a) GO, (b) AuNP and (c) GO-AuNP on lacy carbon coated copper grid. (d-f) HR-TEM images of hybridized composites via the coupling of two platforms, GO-AuNPs and AuNPs via the hybridization of the capture probe sequences with the complementary target sequence. As hybridization happened, AuNPs were found mostly aggregated or linked to each other on GO sheets.

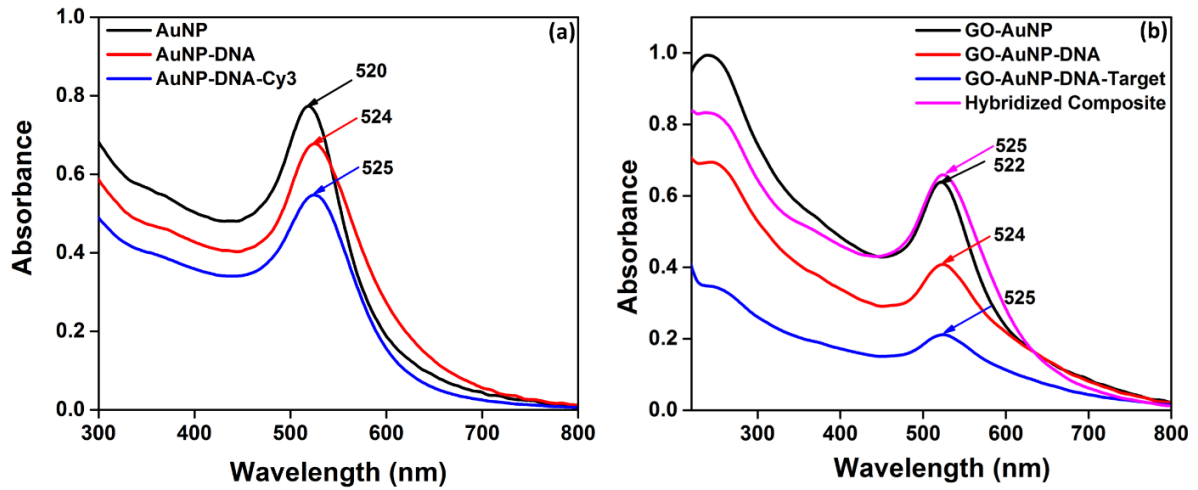


Fig. 3. UV-vis absorption spectra of (a) AuNP, AuNPs-ssDNA and AuNP-ssDNA-Cy3 and (b) GO-AuNPs, GO-AuNPs modified with thiolated CP2, followed by corresponding Target and finally the hybridized composite.

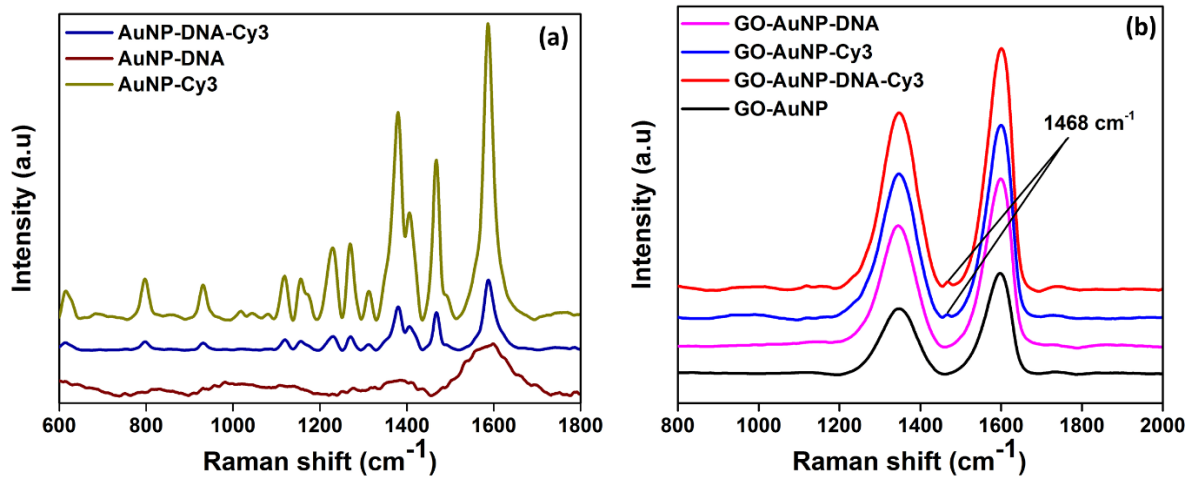


Fig. 4. Raman spectra of AuNPs functionalized with DNA, Cy3 and both DNA and Cy3 (a) GO-AuNP and GO-AuNP functionalized with DNA, Cy3 and both DNA and Cy3 (b).

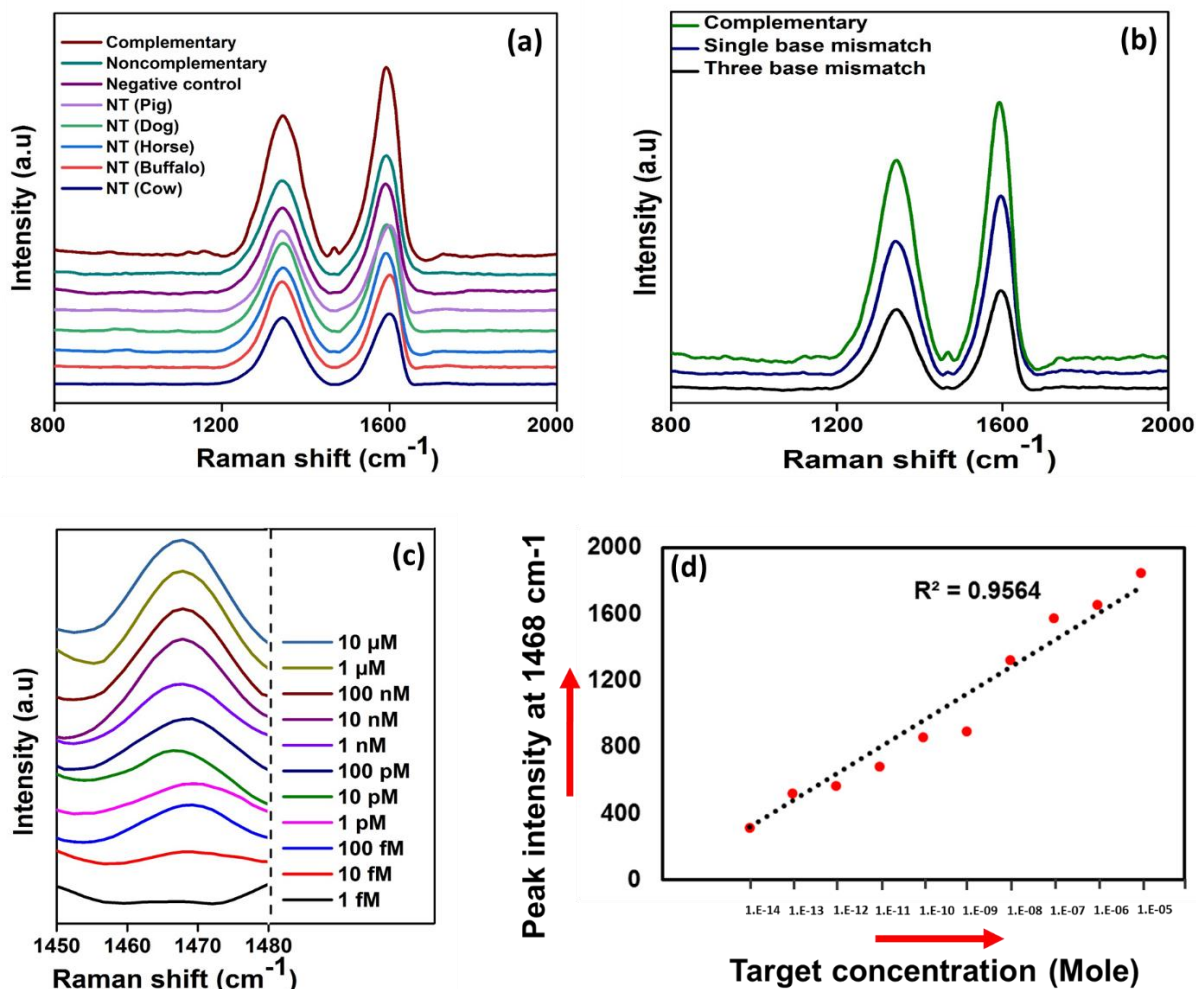


Fig. 5. (a) SERS spectra of the selectivity study. DNA hybridization containing complementary, non-complementary, negative control (blank) and non-Target sequences (pig, dog, horse, buffalo, and cow), and (b) SERS spectra of the biosensor hybridized with corresponding (red), single-base mismatch (dark blue) and three-base mismatches (black) target sequences. (c) Stacked SERS spectra of Cy3 peak at 1468 cm⁻¹ of the composites hybridized with varying concentration of MBT target DNAs (10 μM to 1 fM), displayed from the upper to the lower direction. Here, the spectra were chopped into 1450 to 1480 cm⁻¹ to magnify and distinguish the intensity at peak 1468 cm⁻¹. (d) Linear plot of SERS intensities of 1468 cm⁻¹ band versus corresponding target DNA concentration.

*Highlights (for review)

- A novel and PCR free SERS biosensor was developed for sensitive detection of DNA
- Dual platforms induced hot spots were exploited for the amplified SERS signal.
- The lowest LOD of the fabricated dual-platform sandwich biosensor is 10 fM.
- Short length split-probes were aided to achieve selectivity to single-base mismatch level.

Supplementary Material

[Click here to download Supplementary Material: Supplementary Material.pdf](#)

Declaration of interests

The authors declare that they have no known competing financial interests or personal relationships that could have appeared to influence the work reported in this paper.

The authors declare the following financial interests/personal relationships which may be considered as potential competing interests:

Credit Author Statement

Ibrahim Khalil: Conceptualization, Methodology, Formal analysis, Software, Data curation, Validation, Visualization, Writing - original draft. **Wageeh A. Yehye:** Conceptualization, Funding acquisition, Investigation, Project administration, Resources, Supervision, Writing - review & editing. **Nurhidayatullaili Muhd Julkapli:** Investigation, Supervision, Writing - review & editing. **Shahrooz Rahmati:** Conceptualization, Methodology, Visualization, Software. **Abu Ali Ibn Sina:** Writing - review & editing. **Wan Jeffrey Basirun:** Funding acquisition, Investigation, Supervision. **Mohd Rafie Johan:** Project administration, Resources;

Conflicts of Interest Statement

1
2
3
4
5 **Manuscript title: Graphene oxide and Gold nanoparticle based dual platform with short**
6 **DNA probe for the PCR free DNA biosensing using Surface Enhance Raman Scattering**
7
8
9

10 The authors whose names are listed immediately below certify that they have NO affiliations
11 with or involvement in any organization or entity with any financial interest (such as
12 honoraria; educational grants; participation in speakers' bureaus; membership,
13 employment, consultancies, stock ownership, or other equity interest; and expert testimony
14 or patent-licensing arrangements), or non-financial interest (such as personal or professional
15 relationships, affiliations, knowledge or beliefs) in the subject matter or materials discussed
16 in this manuscript.
17
18
19
20
21
22

Author names:

- 23 1. Ibrahim Khalil
- 24 2. Wageeh A. Yehye
- 25 3. Nurhidayatullaili Muhd Julkapli
- 26 4. Shahrooz Rahmati
- 27 5. Abu Ali Ibn Sina
- 28 6. Wan Jefrey Basirun and
- 29 7. Mohd Rafie Johan
- 30
- 31
- 32
- 33
- 34
- 35
- 36
- 37
- 38
- 39
- 40
- 41
- 42
- 43
- 44
- 45
- 46
- 47
- 48
- 49
- 50
- 51
- 52
- 53
- 54
- 55
- 56
- 57
- 58
- 59
- 60
- 61
- 62
- 63
- 64
- 65